Chapter 11
Phase transitions, cortical gamma, and the selection and read-out of information stored in synapses

J.J. Wright

11.1 Introduction

This chapter attempts a unification of phenomena observable in electrocortical waves, with mechanisms of synaptic modification, learning and recall. In this attempt I draw upon concepts advanced by Freeman and colleagues, and on studies of the mechanism of gamma oscillation in cortex, and of synaptic modification and learning. I use a recently published system of state equations, and numerical simulations, to illustrate the relevant properties.

In Walter Freeman's early work [12, 21], he derived pulse-to-wave and wave-to-pulse conversion equations, and described ensembles of neurons in "K-sets". In recent work [4, 13–20, 22], he has sought a widely embracing theory of perception and cognition by integrating a body of intermediate results, revealing the occurrence of sequential, transiently synchronised and spatially organized electrocortical fields, occurring in the beta and gamma bands, and associated with traveling waves organized into "phase (in the Fourier sense) cones". The origin of these phenomena he and colleagues associate with "phase (in the thermodynamic sense) transitions" in cortical neural activity, marked by signatures in Hilbert-transformed ECoG (electrocorticogram)—termed "phase (in the Fourier sense) slip" and "null spikes".

Freeman's work has features in common with other theoretical approaches [2, 3, 5, 63] but has most in common with those described as mean-field, continuum, or population approximation [26, 41, 66, 68, 75], and is thus in line with the simulation results to be described below.

A large body of other work [7, 8, 11, 23–25, 37, 40, 53, 54] also indicates that gamma oscillation and synchronous oscillation are of central importance. The persuasive link for physiologists, whose emphasis is onunit action potentials, is the

James J. Wright
Liggins Institute, and Department of Psychological Medicine, University of Auckland, Auckland, New Zealand; Brain Dynamics Centre, University of Sydney, Sydney, Australia.
e-mail: jj.w@xtra.co.nz

finding that field potentials and pulse activity are strongly correlated in the gamma frequency band [57]. Yet the mechanisms of origin and the control of gamma oscillation are not fully determined. During gamma oscillation an average lead-vs-lag relation exists between local excitatory and inhibitory cells, as predicted by Freeman [12] and subsequently experimentally observed [27]. Recent analyses of the cellular dynamics [38] conclude that recurrent inhibition from fast-spiking inhibitory cells is largely responsible for maintaining the rhythmic drive—but the role played by excitatory processes in modulating or driving the oscillations remains undetermined. Since cortical networks form a dilute and massively interconnected network, a satisfactory explanation for gamma activity and synchrony should not only consider local dynamics, but also explain the onset and offset of gamma activity in relation to events at more distant sites and at larger scale in the brain, including cortical regulation mediated via subcortical mechanisms. Without clarification of these mechanisms it remains difficult to define the link of gamma activity to information storage, retrieval and transmission, and between thermodynamic and cognitive or informational perspectives.

There are also theoretically important relations of synchrony to information storage and retrieval [32, 33, 44, 67] including recent considerations of synaptic self-organization [72, 73]. These models relate directly or indirectly to wave aspects of cortical signal transmission [8, 9, 29, 37, 45–51, 56, 69, 75]. The present chapter attempts to make these links more explicit, by drawing upon properties demonstrated in a continuum cortical model. Properties of the simulations have been previously reported [70, 71]. A single parameter set obtained *a priori* is used to reproduce appropriate scale-dependent ECoG effects. Receptor dynamics of three major neurotransmitter types and effects of action potential retrograde propagation into the dendritic tree are included, although these features are inessential to the minimalist goal of replication of the ECoG. However, their inclusion assists in linking field properties to information storage and exchange, which is the principal matter to be further explored in the present chapter.

11.2 Basis of simulations

Figures 11.1 and 11.2 show the context of the simulation in relation to qualitative physiological and anatomical features. Crucial anatomical aspects in Fig. 11.1(a) are the local interaction of excitatory (pyramidal) and inhibitory cells in the cortical mantle and extension of the pyramidal tree into the upper cortical layer, to receive nonspecific afferents, while Fig. 11.1(b) sketches the interaction of the cortex with subcortical systems, over recurrent polysynaptic pathways, to regulate the spatial pattern of cortical activation, and hence attentional state [1].

Figure 11.2 indicates microscopic features, and a block diagram of connections, captured in the state equations.

Figure 11.3 shows graphically the steady-state functions, and unit-impulse response functions associated with the simulation parameters. For ease of presentation, the state equations themselves are given in the Appendix (Sect. 11.6.1).
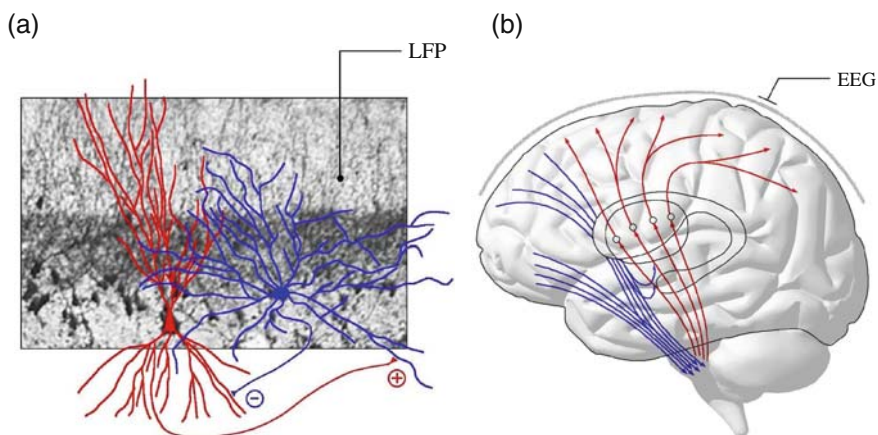
Fig. 11.1 [Color plate] Anatomical aspects of the model. (a) Excitatory (red) and inhibitory (blue) cells in the cerebral cortex. (b) Major cortical and subcortical interactions mediated by descending (blue) and ascending (red) connections. (Reproduced from [71] with permission.)

11.3 Results

11.3.1 Nonspecific flux, transcortical flux, and control of gamma activity

The simulation's state equations and parameter set have the advantage that they can be applied consistently in simulations at two scales—that of a unit macrocolumn about 300 μm across [39]—or that of cortex at the scale of many centimeters, up to the size of the human cortex. In this model, gamma oscillation is defined by analogy to properties of physiological gamma, and comparison of properties at the two scales permits the local effects and the distant influences upon gamma oscillation to be discerned. Effects of parameter variation show that the onset and offset of gamma is subject to variation of all influences upon the excitatory and inhibitory balance, but chief among those influences is the finding that nonspecific flux (NSF) and transcortical flux (TCF) exert opposite effects upon the onset and offset of autonomous gamma oscillation.

At centimetric scale, where longer physiological conduction delays are applied, there is a persistence of stability to higher levels of NSF, in contrast to the macrocolumnar case, with its shorter axonal conduction delays. The two scales of simulation yield a consistent result: increasing levels of uniform NSF over wide extents of cortex suppress the onset of gamma activity. This action of NSF is mediated secondarily by the spread of TCF, which acts upon both excitatory and inhibitory compartments. In contrast, the action of focal NSF, as observed in the macrocolumnar-scale simulations, is to trigger gamma activity, as is next described.
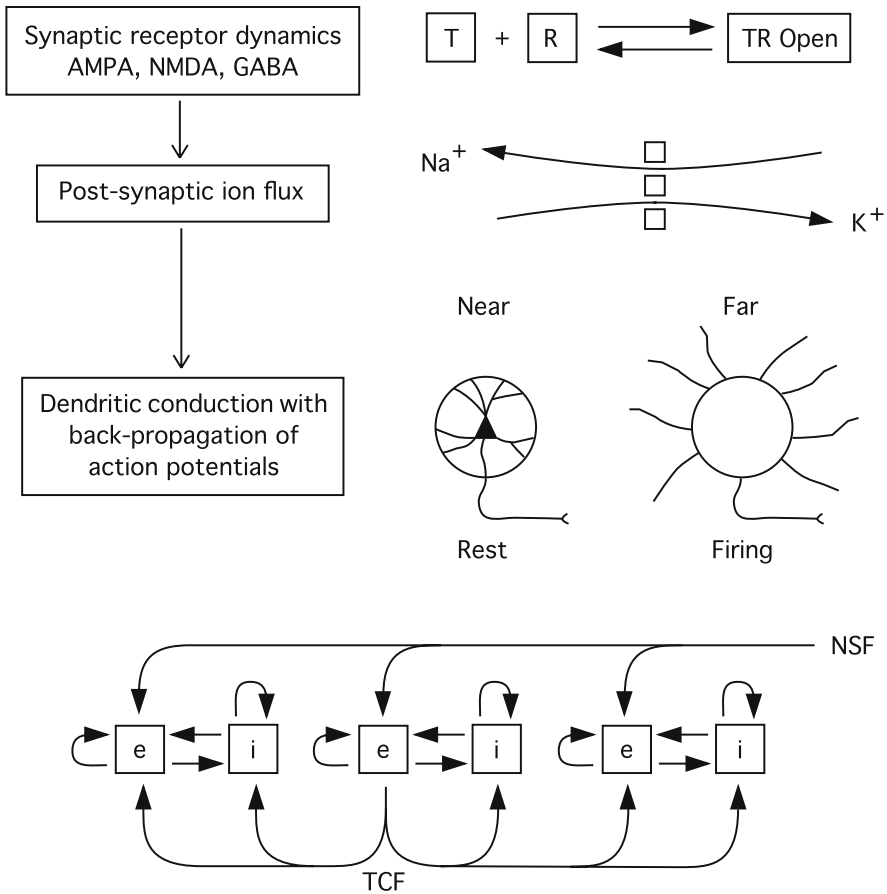
Fig. 11.2 State equations capture the features indicated in descending rows of the figure. (a) Mass-action interaction of neurotransmitters and receptors, thus regulating the opening and closing of ion channels; (b) consequent ionic flux in postsynaptic dendritic membrane; (c) dynamic variation in synaptic weights, consequent to changes in relative and absolute depolarisation of synapses in the proximal and distal dendritic trees, induced by back-propagation of action potentials; (d) cortical architecture, shown in one row of a square array of elements, as blocks of excitatory (*e*) and inhibitory (*i*) cell groups and axo-synaptic linkages. Site of action of the reticular activation system, on *e*-components only, is indicated as NSF (nonspecific flux); the lateral spread of excitatory signals to both *e*- and *i*-components is indicated as TCF (transcortical flux). (Reproduced from [70] with permission.)

11.3.2 Transition to autonomous gamma

Figure 11.4 quantifies the inverse actions of NSF and TCF on the transition to gamma in a macrocolumnar element. It can be seen that the mean value of cell firing increases with NSF, with little sensitivity to TCF. In contrast, over an operating
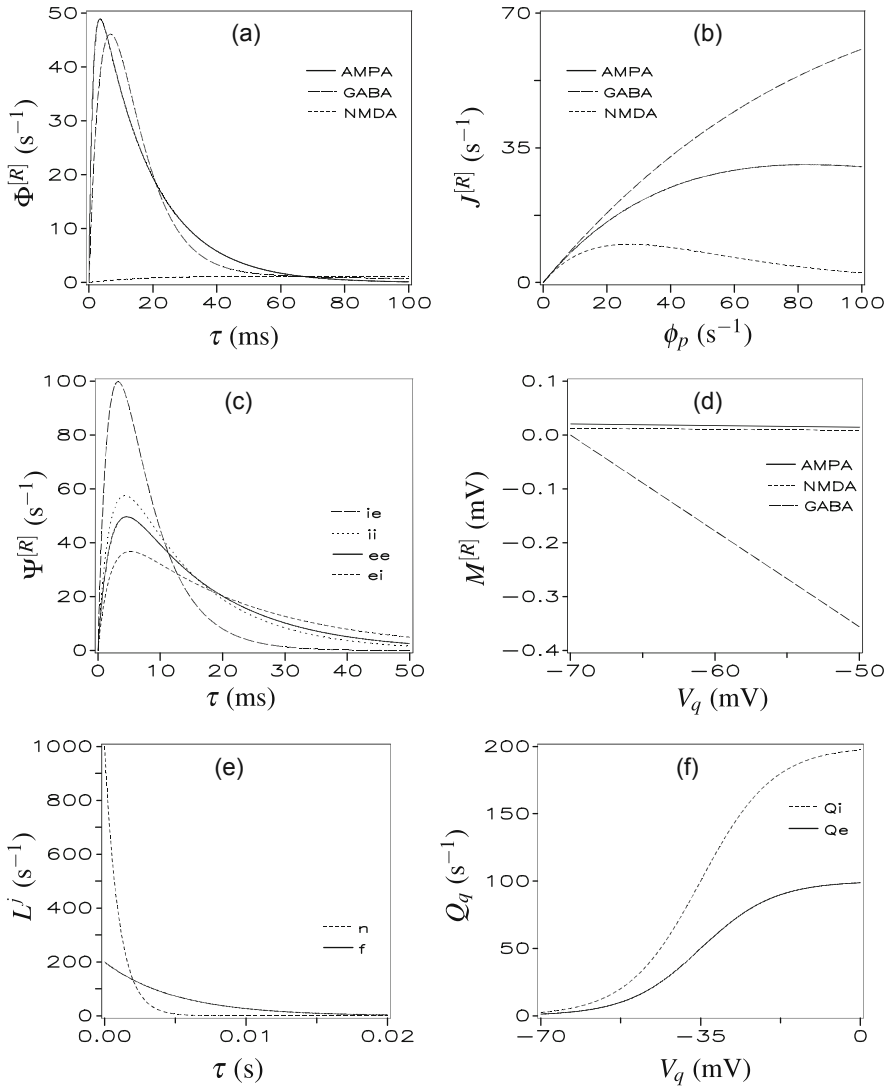
Fig. 11.3 Steady-state and unit-impulse response functions associated with the simulation parameters: (a) normalised receptor time responses; (b) receptor steady states; (c) normalised postsynaptic membrane time responses; (d) postsynaptic membrane steady states at $\phi_p = 20$ s^{-1}; (e) normalised dendritic tree delays; (f) action potential generation. (Reproduced from [70] with permission.)

range of NSF, increasing TCF suppresses autonomous gamma, offering a mechanism for negative feedback between concurrently active patches of cortical gamma oscillation. From lag correlations between the pulse densities of the excitatory and inhibitory compartments of a single element, a measure, $\Theta = 2\pi\,|\ell_+|\,/\,(|\ell_+| + |\ell_-|)$,
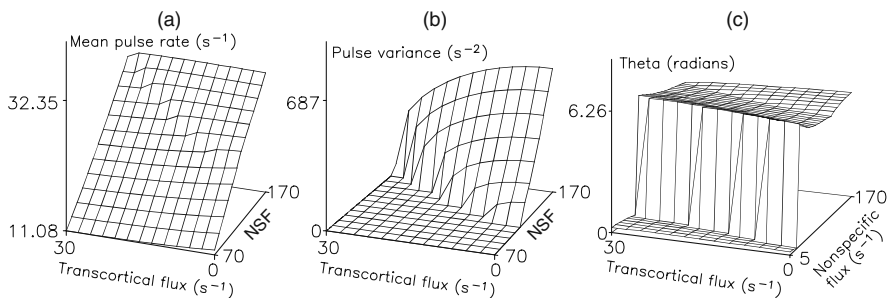
Fig. 11.4 Gamma oscillation as a function of transcortical flux (TCF) and and nonspecific flux (NSF) for macrocolumnar-scale simulations. (a) Mean value of pulse rate in excitatory cells; (b) variance of pulse rate (oscillation power) in excitatory cells; (c) relative phase-lead, Θ, for excitatory vs inhibitory oscillations. (Modified from [70].)

where $|\ell_+|$ and $|\ell_-|$ are the respective lags from zero in the leading and lagging direction to the first peaks in the lag correlation function, was calculated. This measure shows that as the threshold of gamma oscillation is approached, excitatory and inhibitory compartments exhibit lagged correlation over a critical, threshold, range of NSF and TCF. As threshold is exceeded, excitatory and inhibitory compartments begin to fire in phase.

11.3.3 Power spectra

Macrocolumnar scale

Figures 11.5(a, c) show the impact of reciprocal variation of NSF and TCF on the spectrum of gamma oscillation. In all conditions, the spectrum is strongly peaked near the gamma range, with variation from the high-beta range to the high-gamma, with both gamma and high-gamma ($\sim$100 Hz) activity being seen above transition. There is no evidence of a $1/f^2$ spectrum at this scale.

Centimetric scale

Figures 11.5(b, d) show that at centimetric scale and low NSF, a $1/f^2$ spectrum is apparent, and this is greatly enhanced in amplitude when the system is driven by low frequency modulations. As NSF is increased, resonance in the gamma band increases.

11.3.4 Selective resonance near the threshold for gamma oscillation

Figures 11.5 (a, c) show that the spectral form of simulated gamma varies systematically above and below the threshold of transition. To study spectra nearer the
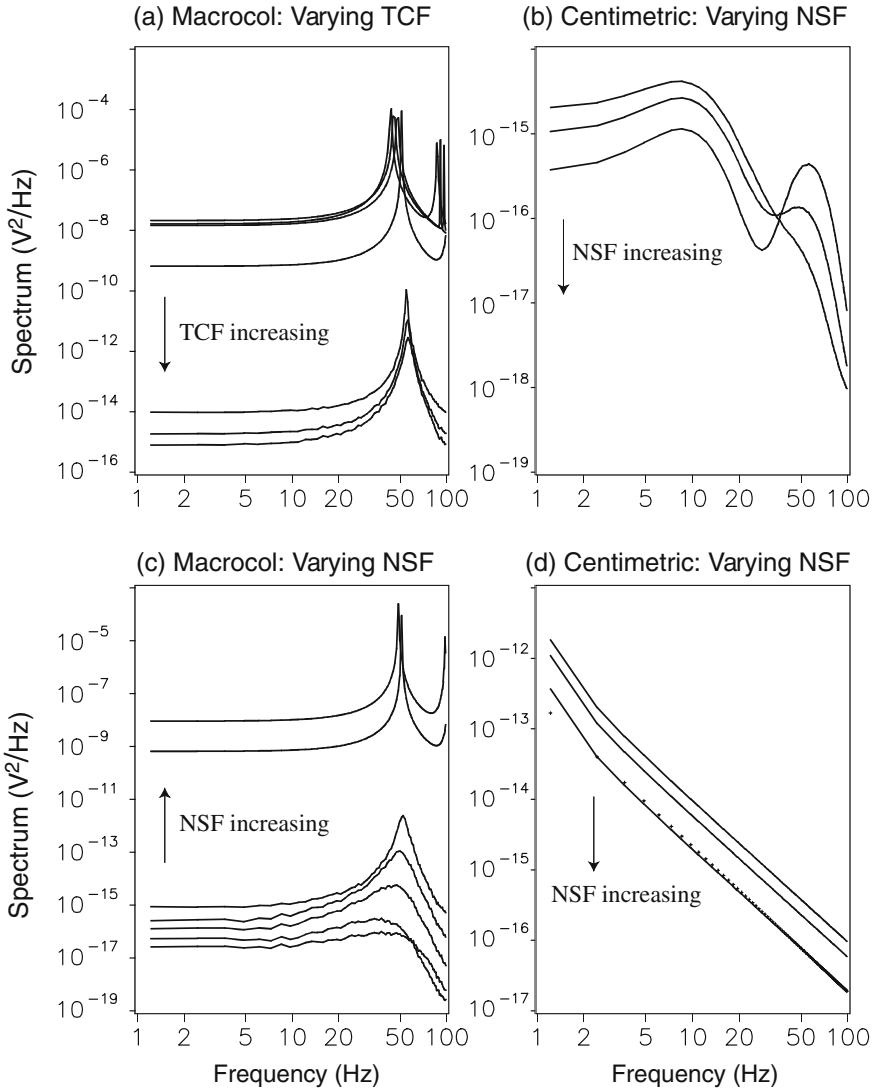
Fig. 11.5 Log-log plots of power spectra at macrocolumnar and centimetric scales. (a) and (c): *Macrocolumnar scale*; upper groups of lines indicate spectra associated with spontaneous oscillation; lower groups of lines indicate spectra for damped resonance. (a) NSF set at 141 s^{-1}; TCF stepped through values 0, 5, 10, 15, 20, 25, 30 s^{-1}, for spectra in order of *decrementing* power at lowest frequencies. (c) TCF set at 15 s^{-1}; NSF stepped through values 0, 28.2, 56.5, 85, 113, 141, 169 s^{-1}, for spectra in order of *incrementing* power at lowest frequencies. (b) and (d): *Centimetric scale*; NSF was set to 0, 8, 16 s^{-1} in order of decrementing power at lower frequencies. (b) Synchronous white-noise input to all elements in the driven row. (d) Driving noise band-limited from 0.002 to 0.954 Hz. Dotted line shows least-squares linear best-fit, with slope −2.07. (Modified from [70].)

transition, power spectra were computed as transition was approached, by applying near-critical levels of NSF. Figure 11.6 shows a representative outcome at macro-columnar scale, with TCF = 15 s^{-1} applied. (Similar results were found at all levels of applied TCF.) It can be seen that as threshold is approached, a broad spectrum centred in the gamma range becomes supplemented by a sharper peak, also in the gamma range. Comparison against the upper curves of Figs. 11.5 (a) and (c) indicates how the sharp gamma peak of sustained oscillation is supplemented by a harmonic in the high gamma range.
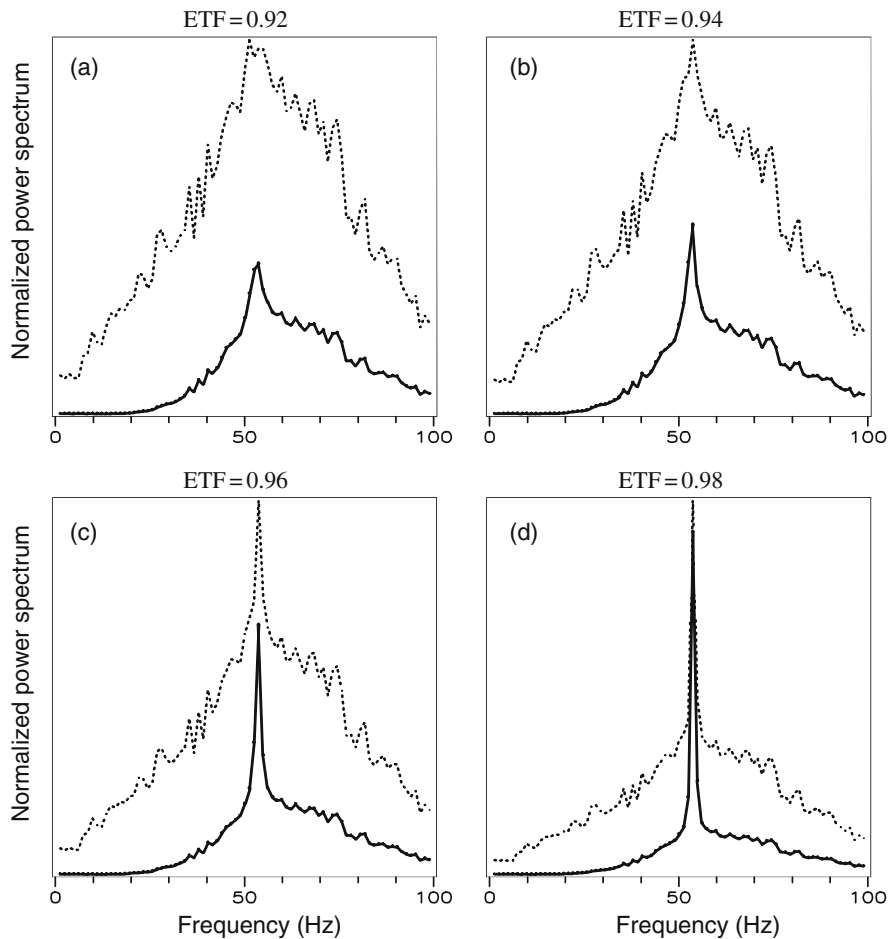

Fig. 11.6 Power spectral response as transition to autonomous gamma activity is approached macrocolumnar scale). Spatiotemporal white noise delivered to all excitatory cell components. ETF = excitatory transition fraction (the fraction of NSF input required to reach threshold for spontaneous oscillation). Solid lines: excitatory compartment; dotted lines: inhibitory compartment. (Reproduced from [71] with permission.)

Figure 11.7 shows firing-rate covariance and phase differences, for centimetric scale, between the excitatory and inhibitory cell continua, during the transition from damped gamma oscillation to autonomous gamma. It can again be seen from the top graph how system sensitivity to small noise inputs increases markedly, while a sharp change in excitatory/inhibitory phase relations characterises the transition, after a premonitory gradual increase in phase difference as transition is approached.
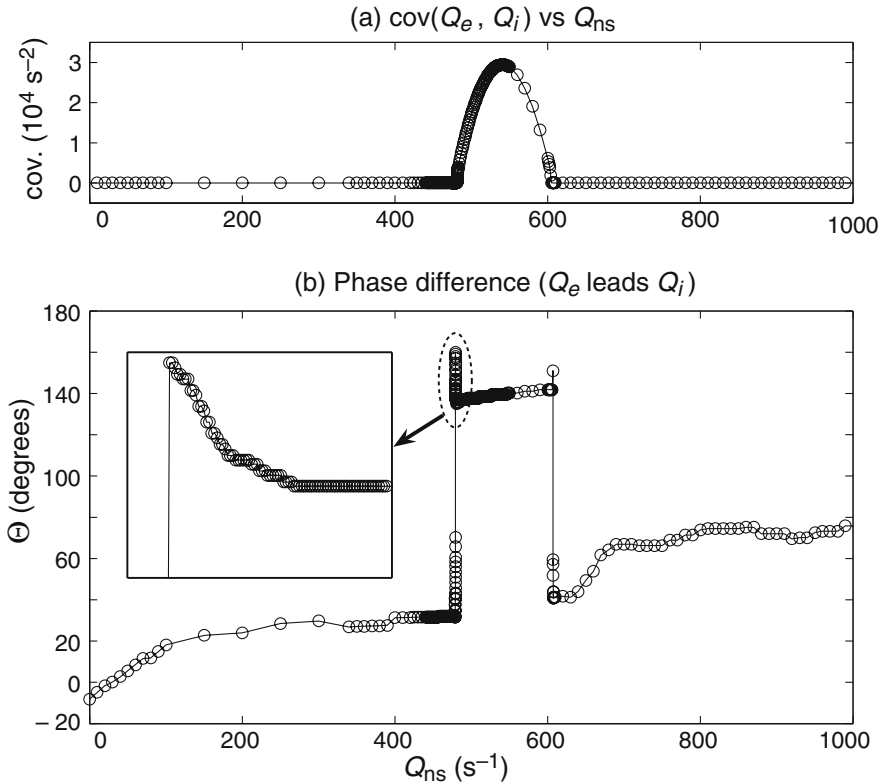

Fig. 11.7 Excitatory/inhibitory covariance and phase relations (centimetric scale) as transition to gamma oscillation is approached and exceeded. Q_{ns} is the level of nonspecific flux (NSF). (a) Zero-lag cross-power of excitatory and inhibitory firing rates at (row-10, col-10) on the cortical sheet; (b) Q_e vs Q_i phase-difference calculated as in Sect. 3.2.

11.3.5 Synchronous oscillation and traveling waves

Two points on a simulated macrocolumn were driven with independent white-noise inputs. Figure 11.8 shows lag covariance between excitatory compartments in two reference elements, adjacent to each of the two driven elements. Amplitudes of the
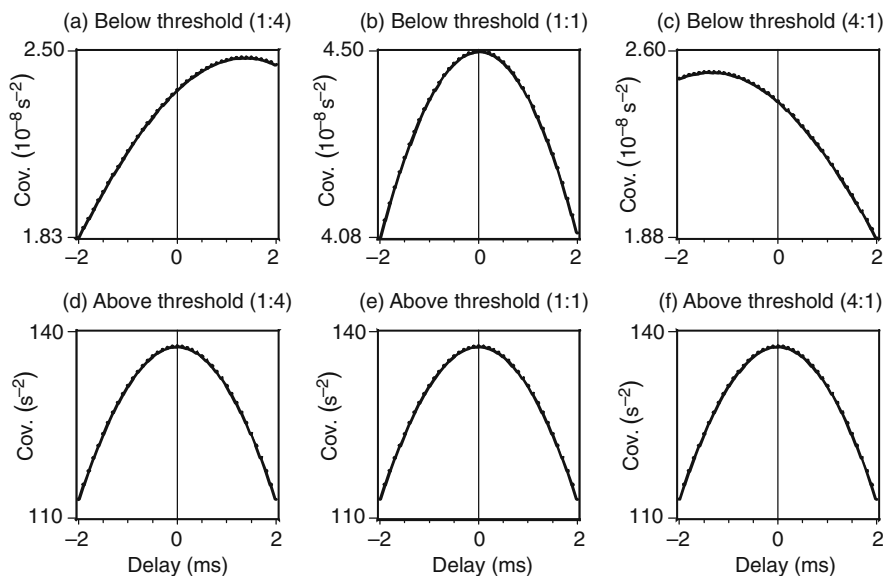
Fig. 11.8 Pulse density covariance versus conduction delay in a macrocolumnar simulation with TCF = 0 s^{-1}. Asynchronous white-noise inputs are delivered to each of two elements, situated at (row, col.) = (10, 16) and (10, 10); lag covariances are computed between elements adjacent to the sites of input. RMS amplitudes of the input signals are in the ratios 1:4, 1:1, 4:1. Top row: Traveling waves apparent below threshold of oscillation (NSF = 61 s^{-1}). Bottom row: Synchronous fields apparent above threshold of oscillation (NSF = 124 s^{-1}). (Modified from [70].)

pair of inputs were adjusted in different runs so that the effect of reversing the ratio of the input amplitudes could be determined.

Below threshold of oscillation, variation of the input amplitudes results in lead and lag between the reference elements, consistent with the passage of traveling waves outwards from the sites of input, while zero-lag synchrony is generated when the input magnitudes are at parity. In the presence of strong oscillation, synchrony is widespread and there is no detectable occurrence of traveling waves despite disparity of input magnitudes. Similar effects appear at centimetric scale except that the lag times of maximum covariance are correspondingly greater, due to the greater axonal conduction lags at the larger scale.

11.4 Comparisons to experimental results, and an overview of cortical dynamics

The limited two-scale results, with their static restraints on NSF and TCF, taken in combination with results from related simulations [9, 47, 48, 74, 76], are consistent with a wide range of experimental findings. The simulation results do not include peaked resonances at the theta, alpha and beta rhythms, the representation

of which requires incorporation of a model of the thalamus [48, 50, 59]. A fuller model would also require consideration of spatiotemporal variation of NSF and TCF.

11.4.1 Comparability to classic experimental data

Simulation results show a good match to widely observed electro-cortical phenomena, despite experimental uncertainties in the values of many parameters, and the use of simplified cortical architecture. The $1/f^2$ background spectrum and the resonance peaks are in accord with EEG in a number of species [8, 18, 43]. The predominance of the $1/f^2$ background when very low frequency inputs are introduced mimics the slow fluctuations in cortical activation associated with variation of the field of attention [1]. There is good correspondence with gamma activity including increasing covariance of pulses and waves as autonomous oscillation is approached [57], and pulse rates accord with those found in awake cortex [55]. Simulation properties shared with related simulations [74], mimic the classic synchrony findings of moving visual-bar experiments [11, 24].

11.4.2 Intracortical regulation of gamma synchrony

It appears that both local and global factors contribute to the control of gamma activity. Locally, all influences on excitatory/inhibitory balance determine specific patterns of firing, while globally the balance of excitatory tone to the excitatory and inhibitory components appears crucial to triggering, and suppressing, gamma activity. A principle aspect of this global control is apparent when it is recalled that NSF was delivered to excitatory cells only, while TCF was delivered to both excitatory and inhibitory components.

A general account of gamma activity and information transfer in the cortex can be advanced by placing the simulation findings at the two scales in their anatomical contexts, as shown in Fig. 11.1. Cortical/subcortical interactions produce a changing pattern of NSF inputs to the cortex, mirrored in the $1/f^2$ background, and facilitating specific spatially organized transitions into autonomous gamma. Patches of autonomous gamma activity inject information into the wider cortical field, leading to the generation of fresh synchronous interactions. Linkages between excitatory cells—including voltage-dependent transmitters—link together patches of gamma activity in synchronous fields, whereas long-range excitatory flux to both excitatory and inhibitory cells (TCF) acts to suppress gamma oscillation, as is shown by the results in Fig. 11.4, (a) and (b), allowing the cortex to self-regulate the onset and offset of gamma activity in complex patterns. The spatial patterning of cortical activation, itself largely controlled by frontal and limbic connections [1], acts to favor particular synchronous fields, thus permitting a large set of possible states of attention. The inclusion of other, slower, cortical resonances in the theta and alpha bands, imposed upon the continuous interaction of time-varying synchronous fields, may be expected to lead to a shutter-like intermittency—as proposed in Freeman's

cinematographic mechanism of perception [17]. The results in Figs. 11.5 and 11.6 show that, near transition levels of NSF, spectral tuning of gamma resonance below threshold, and the spectrum of autonomous gamma above threshold, are well matched, favoring selective information transfer among patches of gamma activity, even if widely separated.

Results in Fig. 11.4(c) are broadly in accord with Freeman's hypothesis of the origin of gamma [12], and help to explain experimental data on inhibitory/excitatory phase relations in gamma [27, 38]. However, these results suggest that gamma oscillation is not merely a simple pendulum-like to-and-fro exchange of excitatory and inhibitory pulses. While phase-lagged activity occurs at intermediate states of excitatory tone, both at low levels of excitation and in states of autonomous oscillation, the excitatory and inhibitory components move into a stable phase relationship with each other. Thus, in the alert state, cortex may be normally poised near transition to oscillation, and sharp changes of excitatory/inhibitory relations may occur when the cortex moves into a locally autonomous mode. Fig. 11.7 emphasises the sudden change of phase at the transition—a change which is literally a "phase slip" (see below). This is consistent with Freeman's concepts of gamma activity as akin to thermodynamic phase transitions—although it is problematic whether phase transition in the formal thermodynamic sense is wholly applicable to a process involving alternation between a linear stochastic state and a nonlinear oscillating state.

11.4.3 Synchrony, traveling waves, and phase cones

The results shown in Figure 11.8 highlight the relationship between traveling waves and synchronous fields by showing that the apparent direction of travel of the waves depends on both the relative magnitude of signal inputs at any two cortical sites and whether or not autonomous, co-operative, oscillations have developed. Directed waves predominate at low levels of cortical excitation, but are no longer observable when swamped by a large zero-lag field as autonomous oscillation supervenes. These effects arise because intersecting cortical traveling waves exhibit annihilation of their anti-phase (odd) components and superposition of their in-phase (even) components [9], resulting in synchrony between equally co-active and reciprocally linked points, generated in times nearly as short as the one-way axonal conduction delay. Waves not intersecting with other co-active sites continue to propagate as pure traveling waves. Figure 11.9 shows the basis of synchrony as a consequence of superposition and cancelation of waves.

The roughly equal numbers of inwardly directed, and outwardly directed radiating waves, identified as phase cones by Freeman and colleagues [13–16, 18, 19], may be the two-dimensional equivalents of the unidirectional traveling waves shown in Fig. 11.8. This interpretation arises from consideration of the self-similar temporal character of the $1/f^2$ background, along with the multicentric variations of NSF supposed to arise from cortical/subcortical interactions. Experimentally and theoretically, electrocortical waves are approximately nondispersive and self-similar
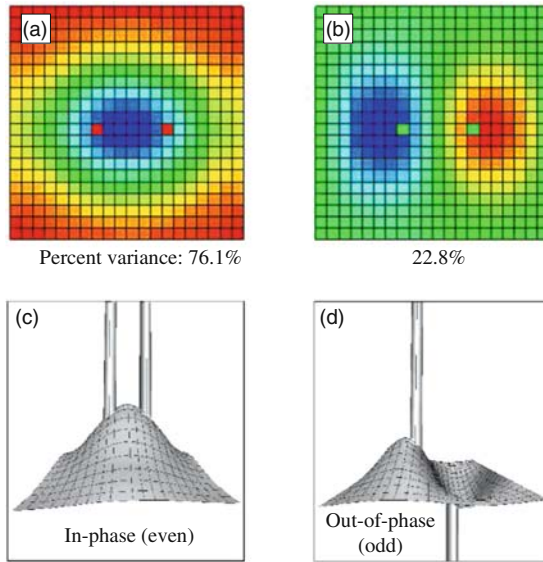
Fig. 11.9 [Color plate] Top row: First and second spatial eigenmodes of waves in a simulated cortical field [33] driven by two independent white-noise time-series of equal variance, applied at the points marked in (a) with red dots. Bottom row: A freeze-frame of motion associated with each eigenmode, showing that the dominant mode (c) arises from summation of inputs of even character at all dendritic summing junctions, while the minor eigenmode (d) arises from reciprocally canceling components.

[13, 43, 77], so there may be self-similarity, or at least considerable spatial complexity, in the fields of autonomous gamma triggered by continuous variation in perception and attention. Depending upon both their scale and position relative to recording electrodes, the fields of synchrony and traveling waves being continually generated and suppressed may be registered as phase cones with traveling wave components radiating either inwards or outwards, as is shown in Fig. 11.10. Association of traveling waves with transient synchronous fields, cone generation at frequencies corresponding to the cerebral rhythms, variation of cone size, origination at multiple foci, association with phase velocities less than, or of similar magnitude to, the conduction velocities of cortical axons, all follow as consequences, and accord with the experimental results. Synchrony, traveling waves, and phase cones.

11.4.4 Phase transitions and null spikes

In recent works Freeman and colleagues [17, 19, 20, 22] have drawn attention to the occurrence of behaviorally linked episodes in ECoG in which analytic power, measured by computing the Hilbert transform, drops to zero, accompanied by a
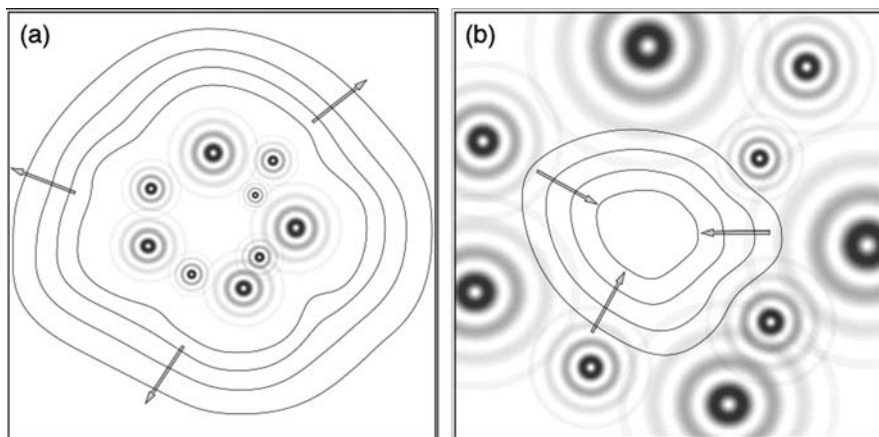
Fig. 11.10 Outwardly- and inwardly-radiating waves generating phase cones. Gray concentric circles represent cortical fields of synchronous oscillation, generated at two scales in a self-similar field of transitions to and from autonomous gamma. Contour lines of similar phase mark average radiation of traveling waves (a) outward, or (b) inward, in surrounding subthreshold field. (Reproduced from [71] with permission.)

sharp step in the accompanying analytic phase. These events they term "null spike", and "phase slip", respectively, and have considered these to be markers of phase transition, in the thermodynamic sense. They also draw attention to the occurrence of similar null spikes in brown noise as a purely random event [22], so it remains uncertain why these apparently random events may be behaviorally linked, and what the association with phase transition actually is.

Figure 11.11 indicates schematically how null spikes and phase slips may be systematically linked to transitions into autonomous gamma activity. The peak of the inverted "Mexican hat" represents a focus on the cortex, which is undergoing a transition into autonomous gamma activity. The spreading transcortical flux stabilizes the surrounding cortex, suppressing oscillation or excursion of the ECoG without significant effect on the average firing rate, as shown in Figs 11.4(a) and (b). This suppression will have the effects of lowering the amplitude, and of reducing the ECoG voltage towards its mean value over time—making zero-crossings of the time-base more likely. At the same time, any ECoG signal recorded from the burst of gamma oscillation occurring at the site of transition may exhibit brief epochs in which the form of the signal is symmetrical about some point in time. These signal characteristics, whether occurring concurrently or not, are each likely to produce an analytic null spike, which therefore has a somewhat ambiguous character since similar events may occur at random. A similar ambiguity may pertain for a phase slip, which might reflect merely the inaccurate calculation of phase near a zero-crossing, or may indicate a sharp change of state like the change from damped resonance to autonomous oscillation. A simple mathematical justification for these deductions is given in the Appendix (Sect. 11.6.2).
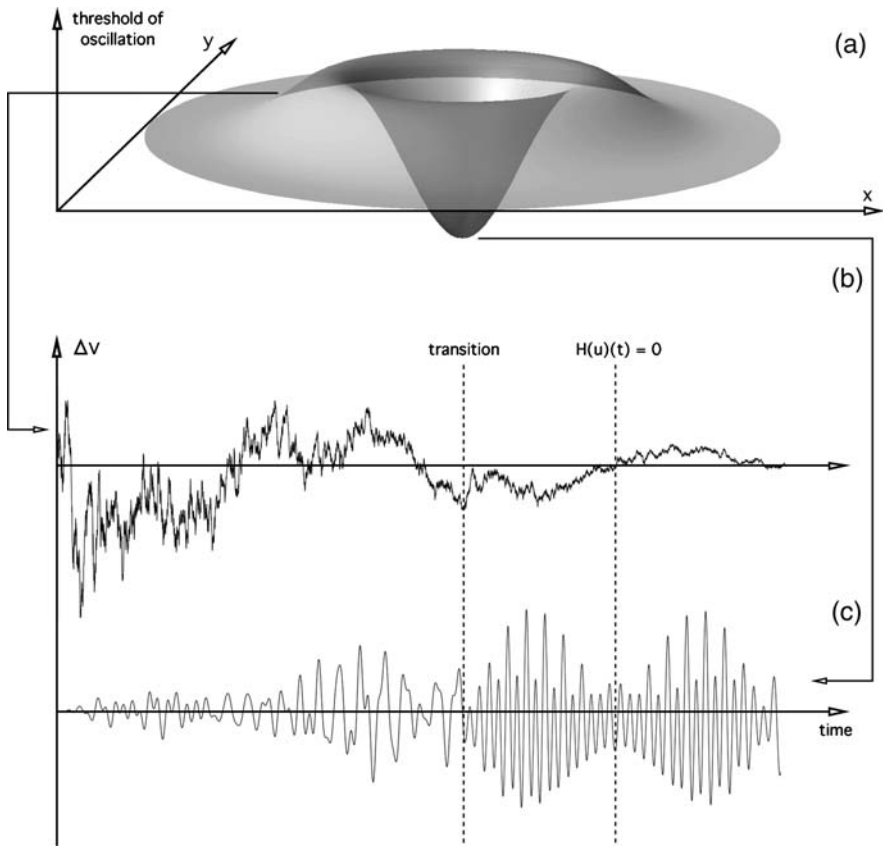
Fig. 11.11 Transition to autonomous gamma, and circumstances combining to favor the occurrence of null spikes and phase slips, measured from ECoG. (a) Schematic representation of the impact of a focus of autonomous gamma, suppressing oscillation in the surrounding field via TCF. (b) ECoG of the surrounding field. Zero-crossing in Gaussian noise favored by the spreading TCF. Zero-mean stochastic background ($1/f^2$ noise) favors $H(u)(t) = 0$ (subject to variation in the time-series sampled). (c) ECoG close to the focus of transition to autonomous gamma. Transition to oscillation with recurrent, time-symmetric character favors $H(u)(t) = 0$, with or without associated zero-crossing. (Reproduced from [71] with permission.)

11.5 Implications for cortical information processing

Preferential selection for input signals in the gamma range as patches of cortex approach transition, and the spectral similarity of the (relatively nonlinear) oscillations in the gamma range, offer a mechanism for tuned information exchange in cortex. The shift to coherent phase relations between excitatory and inhibitory cells, and facilitation of synapses in the far dendritic trees as autonomous gamma is generated, which would permit the ordered readout of information stored in the distal dendritic tree (see Fig. 11.12) while the specific set of inputs sensed in the
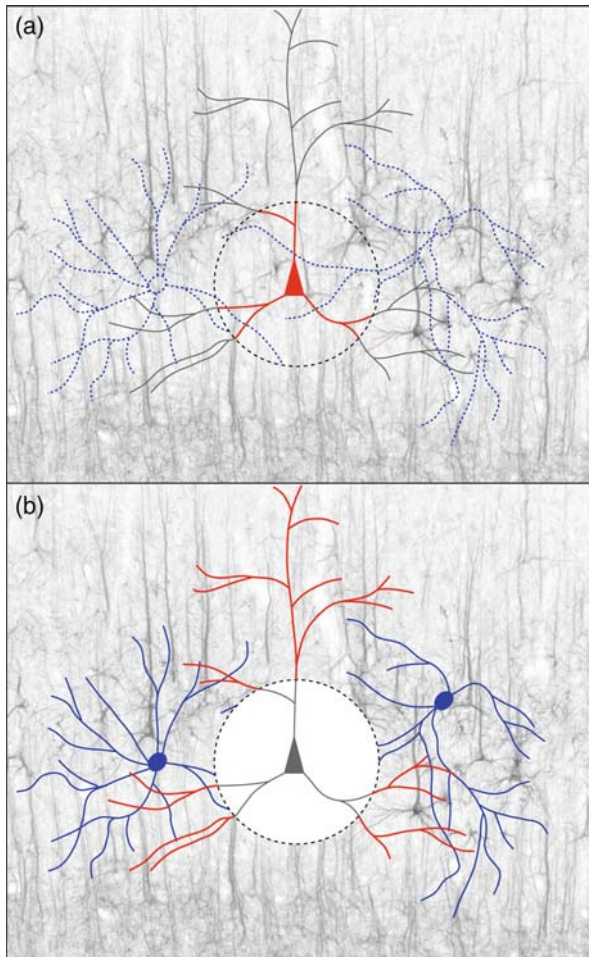
Fig. 11.12 [Color plate] Selection and recall of stored information. (a) Average neuronal state in stochastic background firing conditions. Pyramidal cells (red) are principally susceptible to inputs in the proximal dendritic tree. Inhibitory surround cells (blue) fire with variable timing relative to pyramidal cells. (b) Ordered neuronal state during gamma oscillation. Backpropagating action potentials block proximal synapses. Inhibitory and excitatory cells fire in phase. Synapses of distal dendritic trees mediate spatial and temporal patterns of synchronous oscillation.

proximal dendritic trees would select particular spatiotemporal patterns of synchronous oscillation. These patterns could be very complicated and various, as they draw on synaptic connections in the distal dendritic trees, which are effectively silent until they are brought into play by proximal synapses, which were themselves activated by distant fields of synchronously active cells. The transient synchronous fields, and the traveling wave patterns, can therefore be treated as the

signatures of changes of state in a finite state machine. This raises the important question of whether these dynamic properties can be linked to processes modifying individual synapses, to provide a general model of learning and memory, integrating cognitive activity at both individual cellular and populations scales in the brain.

Recent studies on synaptic modifications in hippocampal cells [31, 64, 65] have led to a distinction between synapses in the proximal dendritic tree, and those in the distal dendritic tree. Those of the proximal tree appear to follow a version of the Hebb rule in which synaptic gain is increased if presynaptic activity precedes postsynaptic, and is decreased if postsynaptic precedes presynaptic. This corresponds to a strengthening of input patterns mediated by one-way transmission—i.e., traveling waves. A second rule, termed the spatiotemporal learning rule (STLR) has been found to apply to the distal dendritic tree, where synapses appear little affected by the postsynaptic state, but mutually facilitate consolidation in neighboring, and coactive, synapses thus favoring the establishment of synapses linking cells engaged in synchronous activity.

The STLR and modified Hebb learning rules correspond in turn to distinctions made in the Coherent Infomax theory advanced by Kay and Phillips and colleagues [32, 33, 44]. This theoretical model also distinguishes two types of synaptic connection—CF connections which are assumed to mediate synchronous activity in adjacent cells, and RF connections, originally named to correspond to receptive field inputs in the visual cortex, but also applicable to any other feed-forward connections. Thus, CF and RF might be equated with synapses on the distal and proximal dendritic trees respectively. Kay and Phillips show that such a network can maximize the storage of information of both individual features transmitted by RF connections, and mutual information transmitted by CF connections, in multiple RF streams. They then show the consolidation of learning requires a learning rule similar to the Hebb rule (although not identical), but can proceed only under the influence of an activation function. The activation function requires that CF activity alone is not sufficient for learning to take place to learn contextual information: cells must be activated by RF connections as well as receiving CF input. Kay and Phillips identify this effect—similar to a gain control—to voltage-sensitive channels of the NMDA type. The idea of activation of the distal dendritic tree by back-propagating action potentials offers a more general mechanism for gain control. Applying the Coherent Infomax concept to more realistic neuronal models, the Relevant Infomax model advanced by Kording and Konig [34] also invokes the effect of back-propagation in the dendritic tree, and distinguishes synapses which largely determine firing from those that gate plasticity—a concept somewhat different from that advanced here.

At present it has not been demonstrated that the physiologically appropriate learning rules and the Coherent Infomax principle can be successfully transplanted to the dynamical model described here. Although the analogies seem clear enough, the information-theoretic ideas have as yet been applied only to small "toy" neuron sets. However, if the concepts do hold for more complex dynamics and connection systems, then a theoretical model of optimised contextual learning, the release of

complex spatiotemporally organized and stored memory sequences, and their relation to electrocortical fields, may be practicable in future.

11.6 Appendix

11.6.1 Model equations

Conventions

State variables are average membrane potentials, $V_{p,q}(\mathbf{r},t)$, pulse densities, $Q_{p,q}(\mathbf{r},t)$, and afferent synaptic flux $\phi_{p,q}(\mathbf{r},t)$. To enable a compact representation, the subscripts $p,q = e,i$ indicate either excitatory (e) or inhibitory (i) neuron populations, while qp indicates synaptic connections from p to q. Superscripts $[R] = $ [NDMA], [AMPA], [GABA$_a$] indicate neurotransmitter receptor types. State equations are steady-state functions of state variables, and lag-response functions in $\tau = n\delta t$, where δt is the time-step, and $n = 1, 2, \ldots$ Lag-response functions are normalised so that $\int_0^\infty f(\tau)\,d\tau = 1$.

Parameter values and references to their derivations are given in Wright (2009) [70, 71] and are based upon largely independent primary and secondary sources [5, 6, 10, 28, 30, 35, 36, 39, 41, 42, 45–47, 52, 55, 58, 60–62].

Afferent synaptic flux

The distribution of the neuron cell bodies giving rise to afferents at a cortical point, $\mathbf{r}$, is $f(\mathbf{r},\mathbf{r}')$, where $\{\mathbf{r}'\}$ are all other points in the field. Connection densities are reciprocal for all $\{\mathbf{r},\mathbf{r}'\}$. The *afferent flux density*, $\phi_p(\mathbf{r},t)$, the population average input pulse rate per synapse, is given by

$$\phi_p(\mathbf{r},t) = \int_0^\infty f(\mathbf{r},\mathbf{r}')\,Q_p(\mathbf{r},t - |\mathbf{r}-\mathbf{r}'|/v_p)\,d^2\mathbf{r}', \qquad (11.1)$$

where $Q_p(\mathbf{r},t)$ are mean pulse rates of neurons at $\mathbf{r}'$, at t, also termed *pulse density*, and v_p is the velocity of axonal conduction. Here, $f(\mathbf{r},\mathbf{r}')$ describes intracortical and cortico-cortical connections, approximated as Gaussian [6]:

$$f(\mathbf{r},\mathbf{r}') = \frac{1}{2\pi\gamma^2}\exp\left(-|\mathbf{r}-\mathbf{r}'|^2/2\gamma^2\right), \qquad (11.2)$$

where γ is the standard deviation axonal range. Equation (11.2) can be applied separately to the short intracortical excitatory and inhibitory fibers, and to the long

range, wholly excitatory, cortico-cortical connections. Steps necessary to compute depolarization as a function of afferent flux density (see Eqs. (11.10) and (11.11)) and the subsequent regeneration of pulses (Eq. (11.12)) are next described.

Transcortical flux (TCF) and nonspecific flux (NSF)

A major distinction is made between the afferent synatic flux transmitted by cortico-cortical fibres, here termed the *transcortical flux* (TCF; see Fig. 11.2), and excitatory synaptic flux delivered wholly to the excitatory cortical cells, from the reticular activation system, and termed *nonspecific afferent flux* (NSF; see Fig. 11.2). In the macrocolumnar-scale simulations, NSF is introduced by adding a given value of synaptic flux, in spikes per second, weighted by $N_{ee,ns}/N_{TOT}$, the fraction of synapses per excitatory cortical cell attributable to subcortical afferents, to $Q_e(\mathbf{r},t)$, the pulse densities of the excitatory cells.

Synaptic receptor dynamics

The postsynaptic impact of $\phi_p(\mathbf{r},t)$ is modified by changes in the conformation of ion channels. The open-channel steady state is

$$J^{[R]}(\phi_p) = \exp\left(-\lambda^{[R]}\phi_p\right)\phi_p, \tag{11.3}$$

and $\Phi^{[R]}(\tau)$ describes the rise and fall of receptor adaptation to a brief afferent stimulus

$$\Phi^{[R]}(\tau) = \left[\sum_n B_n^{[R]}/\beta_n^{[R]} - \sum_m A_m^{[R]}/\alpha_m^{[R]}\right]^{-1} \times$$
$$\left[\sum_n B_n^{[R]}\exp\left(-\beta_n^{[R]}\tau\right) - \sum_m A_m^{[R]}\exp\left(-\alpha_m^{[R]}\tau\right)\right], \tag{11.4}$$

where $\{\lambda^{[R]}, B_n^{[R]}, A_m^{[R]}, \beta_n^{[R]}, \alpha_m^{[R]}\}$ with $m,n = 1,2,3\ldots$, are derived from transmitter/receptor models.

Postsynaptic membrane gain

Afferent synaptic flux, modified by synaptic adaptation, generates a change in average membrane potential, V_q, with a steady state solution

$$M^{[R]}(V_q,\phi_p) = g_p^{[R]}\left(\frac{V_p^{rev} - V_q}{V_p^{rev} - V_q^{[0]}}\right) J^{[R]}. \tag{11.5}$$

Here, $g_p^{[R]}$ is the synaptic gain at resting membrane potential, V_p^{rev} is the excitatory or inhibitory reversal potential, and $V_q^{[0]}$ is the resting membrane potential. Since V_q and ϕ_p are serially-dependent state variables, $V_q(t)$ must be substituted by $V_q(t - \delta t)$ in computation.

Dendritic time- and space-response

The rise and fall of postsynaptic membrane potential at the sites of synaptic input is given by,

$$\Psi^{[R]}(\tau) = \frac{a_{qp}b_{qp}}{b_{qp} - a_{qp}} \left(\exp[-a_{qp}\tau] - \exp[-b_{qp}\tau] \right), \qquad (11.6)$$

where $\{a_{qp}, b_{qp}\}$ are constants. Postsynaptic depolarization, transferred by cable effects, reaches the action potential trigger points after delays which are greater from synapses in the distal dendritic trees that from proximal dendritic trees. The relative magnitudes of depolarization reaching the trigger points over a spread of arrival times is given by,

$$L^j(\tau) = \mathscr{A}^j \exp[-\mathscr{A}^j\tau]. \qquad (11.7)$$

The $\mathscr{A}^j$ are constants, and $j = n, f$ indicates relationship to the near or far dendritic trees respectively.

Effects of action potential back-propagation

At the release of an action potential, anterograde and retrograde propagation takes place, the latter depolarizing the membrane throughout the proximal dendritic tree [58]. It is assumed that when the neuron is fully repolarized, the greatest weight in the generation of a subsequent action potential can be ascribed to activity at the near synapses, because of their weighting by proximity to the axon hillock. On the release of an action potential, the near synapses become reduced in efficacy to zero during the absolute refractory period, and the distal synaptic trees become partially depolarized, so that determination of whether or not a subsequent action potential is generated at the conclusion of the relative refractory period is then relatively weighted toward activity at the far synapses.

The fractions of neurons A^n, A^f, having respective biases toward activation from the near or far dendritic trees, are

$$A^f(t) = Q_q(t)/Q_q^{\text{max}}, \qquad (11.8)$$

$$A^n(t) = 1 - Q_q(t)/Q_q^{\text{max}}, \qquad (11.9)$$

where Q_q^{max} is the maximum firing rate of neurons and reflects the refractory period.

Fractional distributions, $r^{n[R]} + r^{f[R]} = 1$, of postsynaptic receptors of each type, differ in near and far trees, so back-propagation also influences the efficacy of receptor types, and the voltage dependence on NMDA receptors requires that they be considered as essentially components of the distal tree, with $r^{f[\mathrm{NMDA}]} = 1$.

Aggregate depolarization

The voltage at the trigger points for action potential generation, ψ_q, is obtained by convolution and summation over the receptor types, excitatory/inhibitory cell combinations, and fractions of quiescent and recently active cells, weighted by the average number of synaptic connections between cell types, N_{qp},

$$\psi_q(t) = \sum_p \sum_j \sum_{[R]} N_{qp} A^j r^{j[R]} \left(\left((M^{[R]} \otimes \Phi^{[R]}) \otimes \Psi^{[R]} \right) \otimes L^j \right), \qquad (11.10)$$

where $\otimes$ indicates convolution in time. In the population average,

$$V_q(t) \approx V_q^{[0]} + \psi_q(t). \qquad (11.11)$$

Equation (11.11) establishes $V_q(t - \delta t)$ for the next time-step in Eq. (11.5).

Action potential generation

From Eq. (11.11), the mean firing rate is calculated from

$$Q_q(t) = Q_q^{\mathrm{max}} / (1 + \exp[-\pi(V_q - \theta_q)/\sqrt{3}\sigma_q]), \qquad (11.12)$$

yielding the pulse densities of neurons required in Eq. (11.1). Here, θ_q is the mean value of of V_q at which 50% of neurons are above threshold for the emission of action potentials; and σ_q approximates one standard deviation of probability of emission of an action potential in a single cell, as a function of V_q. For a comparison with standard EEG and local field potential (LFP) data, we also assume $\mathrm{LFP} \equiv V_e(t)$.

Application at mesoscopic (macrocolumnar) and macroscopic (centimetric) spatial scales

The above equations are applied numerically in spatially discrete form, in a 20×20 grid of "elements", with periodic boundary conditions. Each element of the grid is situated at position $\mathbf{r}$, surrounded by other elements at positions $\{\mathbf{r}'\}$, coupled as in Eq. (11.1) with delays, $\delta_p = |\mathbf{r} - \{\mathbf{r}'\}|/v_p$, and $f(\mathbf{r}, \{\mathbf{r}'\})$ chosen as the sum of two-dimensional Gaussian distributions of connections, each Gaussian term appropriate to intracortical and cortico-cortical connections, of excitatory and inhibitory types. The grid can be used to represent the cortex at any chosen spatial scale, by applying

a physiologically appropriate value for v_p, and setting excitatory/inhibitory axonal connection ranges appropriate to scale. Two configurations are used:

- a centimetric scale, which treats inhibitory and short intracortical connections as local to each element, with cortico-cortical connections linking elements. Non-specific afferent flux (NSF) is applied uniformly to all excitatory elements, and thus provides a single control parameter;
- a macrocolumnar scale, which connects elements together by both intracortical excitatory and inhibitory connections, forming a "Mexican hat" connection field of approximately 300-μm diameter. At this scale, no cortico-cortical connections are represented explicitly. Instead, the transcortical flux is introduced as a spatially uniform input to all elements of the simulation. Thus, at macrocolumnar scale, there are two control parameters—the nonspecific flux (NSF), and the transcortical flux (TCF).

Numerical considerations

Simulation time-step was 0.1 ms. Individual simulation runs were considered to have reached a statistically stationary state at $t = 200$ s after initialization with state variables set to zero. The final 0.8192 s of each simulation run was used to determine whether the final state was steady state (negligible power other than at DC) or one of oscillation. Single runs were used for all estimates in which external noise was not applied. With the application of noise-like driving signals, ensembles of $\sim$100 independently obtained 0.8192-s final epochs were analyzed for all spectral and correlation analyses. Noise inputs were applied as zero-mean signals added to the applied constant values of NSF, and unless otherwise stated, were applied to the top row (row-0) of the simulated grid of units, while excitatory cell potentials were recorded from the element at row-10, column-10.

Simulated gamma oscillation was defined as oscillation with a peak frequency in the 30–60-Hz band, associated with a threshold reached with increasing NSF producing transition from a static steady-state (in the absence of noise) or dampened oscillation (in the presence of driving noise), to an autonomous oscillation, with the transition occurring below a mean excitatory firing rate of 20 s^{-1}, and not associated with excursions of membrane potential encountering reversal-potential bounds. Normal firing patterns of cortical neurones other than gamma were equated with stochastic background and identified with the simulation's non-oscillating states.

11.6.2 Hilbert transform and null spikes

The Hilbert transform is given by

$$H(u)(t) = -\frac{1}{\pi}\lim_{\varepsilon \downarrow 0}\int_{\varepsilon}^{\infty}\frac{u(t+\tau')-u(t-\tau')}{\tau'}d\tau', \qquad (11.13)$$

where $u(t)$ is a stationary, continuous, and infinite-duration signal, and τ' is the temporal lag. In a discrete approximation for a time-limited epoch,

$$H(u)(t) = \frac{1}{\pi} \sum_{\tau=1}^{m} \frac{u(t+\tau) - u(t-\tau)}{\tau} \qquad (11.14)$$

where t is now a dimensionless time-index, $\tau = \tau'/\varepsilon$, ε is the time-step, and m is the number of forward time-steps in the epoch. Let $\bar{u}(t)$ be the mean value of the set $S \equiv \{u(t+\tau) - u(t-\tau)\}$, and let

$\{\tilde{u}(t,\tau)\} \subseteq S$ be the subset whose members are equal to $\bar{u}(t)$,
$\{\hat{u}(t,\tau)\} \subseteq S$ be the subset whose members are each greater than $\bar{u}(t)$,
$\{\breve{u}(t,\tau)\} \subseteq S$ be the subset whose members are each less than $\bar{u}(t)$,

then let $\sum \tilde{u}(t,\tau)/\tau$, $\sum \hat{u}(t,\tau)/\tau$, $\sum \breve{u}(t,\tau)/\tau$ be the sums of terms, each weighted by τ, in the respective subsets. Thus,

$$H(u)(t) = \frac{1}{\pi} \left(\sum \frac{\tilde{u}(t,\tau)}{\tau} + \sum \frac{\hat{u}(t,\tau)}{\tau} + \sum \frac{\breve{u}(t,\tau)}{\tau} \right). \qquad (11.15)$$

Special cases in which $H(u)(t) = 0$ are:

1. For all $\tau \geq \varepsilon$, $u(t+\tau) = u(t-\tau)$, hence

$$\sum \tilde{u}(t,\tau)/\tau = \sum \hat{u}(t,\tau)/\tau = \sum \breve{u}(t,\tau)/\tau = 0; \qquad (11.16)$$

2. When elements of S are randomly distributed about $\bar{u}(t)$, with $\bar{u}(t) = 0$, hence

$$\sum \hat{u}(t,\tau)/\tau = -\sum \breve{u}(t,\tau)/\tau, \quad \text{and} \quad \sum \tilde{u}(t,\tau)/\tau = 0. \qquad (11.17)$$

Therefore analytic power, $H^2(u)(t) + u^2(t)$, can approach zero where:

1. $u(t)$ is symmetric about some t, and $u(t) \to 0$; (this includes the special case where $u(t) = 0$ for all t);
2. $u(t)$ is close to or identical with a zero-crossing in a sample of a zero-mean Gaussian noise.

Analytic phase, $\tan^{-1}[H(u)(t)/u(t)]$, is ill-defined where $u(t) \to 0$, but a sharp change in analytic phase might also be detected in association with physiological equivalent of the step-like transition shown in Fig. 11.7.

References

1. Alexander, G.E., Crutcher, M.D., DeLong, M.R.: Basal ganglia-thalamocortical circuits: Parallel substrates for motor, oculomotor, prefrontalâ and limbic functions. In: H.B.M. Uylings (ed.), The Prefrontal Cortex: Its Structure, Function, and Pathology, Elsevier, Amsterdam (1990)
2. Amit, D.J.: Modelling Brain Function. Cambridge University Press, Cambridge (1989)

3. Arbib, M.A. (ed.): The Handbook of Brain Theory and Neural Networks. MIT Press, Cambridge, Massachussetts (1995)

4. Barrie, J.M., Freeman, W.J., Lenhart, M.D.: Spatiotemporal analysis of prepyriform, visual, auditory, and somesthetic surface EEGs in trained rabbits. J. Neurophysiol. **76**, 520–539 (1996)

5. Bower, J., Beeman, D.: The Book of GENESIS. Exploring Realistic Neural Models with the GEneral NEural SImulation System. Springer, New York, 2nd edn. (1998)

6. Braitenberg, V., Schuz, A.: Anatomy of the Cortex: Statistics and Geometry. Springer-Verlag, Berlin, New York (1991)

7. Bressler, S.L., Coppola, R., Nakamura, R.: Episodic multiregional cortical coherence at multiple frequencies during visual task performance. Nature **366**, 153–156 (1993), doi:10.1038/366153a0

8. Buzsaki, G., Draguhn, A.: Neuronal oscillations in cortical networks. Science **304**, 1926–1929 (2004), doi:10.1126/science.1099745

9. Chapman, C.L., Bourke, P.D., Wright, J.J.: Spatial eigenmodes and synchronous oscillation: Coincidence detection in simulated cerebral cortex. J. Math. Biol. **45**, 57–78 (2002), doi:10.1007/s002850200141

10. Dominguez-Perrot, C., Feltz, P., Poulter, M.O.: Recombinant GABAa receptor desensitization: The role of the gamma2 subunit and its physiological significance. J. Physiol. **497**, 145–159 (1996)

11. Eckhorn, R., Bauer, R., Jordon, W., Brosch, M., Kruse, W., Monk, M., Reitboeck, H.J.: Coherent oscillations: A mechanism of feature linking in the in the visual cortex? Biol. Cybern. **60**, 121–130 (1988), doi:10.1007/BF00202899

12. Freeman, W.J.: Predictions on neocortical dynamics derived from studies of paleocortex. In: Induced Rhythms of the Brain, Birkhauser, Boston (1991)

13. Freeman, W.J.: Origin, structure and role of background EEG activity. Part 1: Analytic amplitude. Clin. Neurophysiol. **115**, 2077–2088 (2004), doi:10.1016/j.clinph.2004.02.029

14. Freeman, W.J.: Origin, structure and role of background EEG activity. Part 2: Analytic phase. Clin. Neurophysiol. **115**, 2089–2107 (2004), doi:10.1016/j.clinph.2004.02.028

15. Freeman, W.J.: Origin, structure and role of background EEG activity. Part 3: Neural frame classification. Clin. Neurophysiol. **116**, 1118–1129 (2005), doi:10.1016/j.clinph.2004.12.023

16. Freeman, W.J.: Origin, structure and role of background EEG activity. Part 4: Neural frame simulation. Clin. Neurophysiol. **117**, 572–589 (2006), doi:10.1016/j.clinph.2005.10.025

17. Freeman, W.J.: Proposed cortical 'shutter' mechanism in cinematographic perception. In: L.I. Perlovsky, R. Kozma (eds.), Neurodynamics of Cognition and Consciousness, pp. 11–38, Springer, Heidelberg (2007), doi:10.1007/978-3-540-73267-9_2

18. Freeman, W.J., Barrie, J.M.: Analysis of spatial patterns of phase in neocortical gamma EEGs in rabbit. J. Neurophysiol. **84**, 1266–1278 (2000)

19. Freeman, W.J., Holmes, M.D., West, G.A., Vanhatalo, S.: Fine spatiotemporal structure of phase in human intracranial EEG. Clin. Neurophysiol. **117**, 1228–1243 (2006), doi:10.1016/j.clinph.2006.03.012

20. Freeman, W.J., Vitiello, G.: Dissipation and spontaneous symmetry breaking in brain dynamics. J. Phys. A: Gen. Phys. **41**, 17p (2008), doi:10.1088/1751-8113/41/30/304042

21. Freeman, W.: Mass Action in the Nervous System. Academic Press, New York (1975)

22. Freeman, W., O'Nuillain, S., Rodriguez, J.: Simulating cortical background activity at rest with filtered noise. J. Integr. Neurosci. **7**(3), 337–344 (2008), doi:10.1142/S0219635208001885

23. Gray, C.M., Engel, A.K., Konig, P., Singer, W.: Synchronization of oscillatory neuronal responses in cat striate cortex: Temporal properties. Vis. Neurosci. **8**, 337–347 (1992)

24. Gray, C.M., Konig, P., Engel, A.K., Singer, W.: Oscillatory responses in cat visual cortex exhibit intercolumnar synchronisation which reflects global stimulus properties. Nature **388**, 334–337 (1989), doi:10.1038/338334a0

25. Gray, C.M., Singer, W.: Stimulus-specific neuronal oscillations in orientation columns of cat visual cortex. Proc. Natl. Acad. Sci. U.S.A. **86**, 1698–1702 (1989), doi:10.1073/pnas.86.5.1698

26. Haken, H.: Principles of Brain Functioning. Springer, Berlin (1996)

27. Hasenstaub, A., Shu, Y., Haider, B., Kraushaar, U., Duque, A., McCormick, D.A.: Inhibitory postsynaptic potentials carry synchronized frequency information in active cortical networks. Neuron **47**, 423–435 (2005), doi:10.1016/j.neuron.2005.06.016

28. Hausser, W., Roth, A.: Dendritic and somatic glutamate receptor channels in rat cerebellar purkinje cells. J. Physiol. **501**, 77–95 (1997), doi:10.1111/j.1469-7793.1997.077bo.x

29. Jirsa, V.K., Haken, H.: Field theory of electromagnetic brain activity. Phys. Rev. Lett. **77**, 960–963 (1996), doi:10.1103/PhysRevLett.77.960

30. Kandel, E.R., Schwartz, J.H., Jessell, T.M.: Principles of Neural Science. Prentice-Hall International, London, 3 edn. (1991)

31. Kaneki, K., Ariki, O., Tsukada, M.: Dual synaptic plasticity in the hippocampus: Hebbian and spatiotemporal learning dynamics. Cogn. Neurodyn. **(in Press)** (2008), doi:10.1007/s11571-008-9071-z

32. Kay, J., Floreano, D., Phillips, W.A.: Contextually guided unsupervised learning using local multivariate binary processors. Neural Netw. **11**(1), 117–140 (1998), doi:10.1016/S0893-6080(97)00110-X

33. Kay, J., Phillips, W.A.: Activation functions, computational goals and learning rules for local processors with contextual guidance. Neural Comp. **9**, 763–768 (1997), doi:10.1162/neco.1997.9.4.895

34. Kording, K.P., Konig, P.: Learning with two sites of synaptic integration. Network: Comp. Neural Sys. **11**, 25–39 (2000), doi:10.1088/0954-898X/11/1/302

35. Lester, R.A., Jahr, C.E.: NDMA channel behavior depends on agonist affinity. J. Neurosci. **12**, 635–643 (1992)

36. Liley, D.T.J., Wright, J.J.: Intracortical connectivity of pyramidal and stellate cells: Estimates of synaptic densities and coupling symmetry. Network: Comp. Neural Sys. **5**, 175–189 (1994), doi:10.1088/0954-898X/5/2/004

37. Miltner, W.H., Braun, C., Arnold, M., Witte, H., Taube, E.: Coherence of gamma-band EEG activity as a basis for associative learning. Nature **397**, 434–436 (1999), doi:10.1038/17126

38. Morita, K., Kalra, R., Aihara, K., Robinson, H.P.C.: Recurrent synaptic input and the timing of gamma-frequency-modulated firing of pyramidal cells during neocortical "up" states. J. Neurosci. **28**, 1871–1881 (2008), doi:10.1523/JNEUROSCI.3948-07.2008

39. Mountcastle, V.B.: An organizing principle for cerebral function: The unit module and the distributed system. In: The Neurosciences 4th Study Program, MIT Press, Cambridge, Mass (1979)

40. Neuenschwander, S., Singer, W.: Long-range synchronisation of oscillatory light responses in the cat retina and lateral geniculate nucleus. Nature **379**, 728–733 (1996), doi:10.1038/379728a0

41. Nunez, P.L.: Electric Fields of the Brain. Oxford University Press, New York (1981)

42. Nunez, P.L.: Neocortical Dynamics and Human EEG Rhythms. Oxford University Press, New York (1995)

43. O'Connor, S.C., Robinson, P.A.: Wave-number spectrum of electrocorticographic signals. Phys. Rev. E **67**, 1–13 (2003), doi:10.1103/PhysRevE.67.051912

44. Phillips, W.A., Singer, W.: In search of common foundations for cortical computation. Behav. Brain Sci. **20**, 657–722 (1997), doi:10.1017/S0140525X9700160X

45. Rennie, C.J., Robinson, P.A., Wright, J.J.: Effects of local feedback on dispersion of electrical waves in the cerebral cortex. Phys. Rev. E **59**, 3320–3329 (1999), doi:10.1103/PhysRevE.59.3320

46. Rennie, C.J., Robinson, P.A., Wright, J.J.: Unified neurophysical model of EEG spectra and evoked potentials. Biol. Cybern. **86**, 457–471 (2002), doi:10.1007/s00422-002-0310-9

47. Rennie, C.J., Wright, J.J., Robinson, P.A.: Mechanisms of cortical electrical activity and the emergence of gamma rhythm. J. Theoretical. Biol. **205**, 17–35 (2000), doi:10.1006/jtbi.2000.2040

48. Robinson, P.A., Rennie, C.J., Rowe, D.L., O'Connor, S.C., Wright, J.J., Gordon, E.: Neurophysical modelling of brain dynamics. Neuropsychopharmacol. **28**, S74–S79 (2003), doi:10.1038/sj.npp.1300143

49. Robinson, P.A., Rennie, C.J., Wright, J.J.: Propagation and stability of waves of electrical activity in the cerebral cortex. Phys. Rev. E **56**, 826–840 (1997), doi:10.1103/PhysRevE.56.826

50. Robinson, P.A., Rennie, C.J., Wright, J.J., Bahramali, H., Gordon, E., Rowe, D.L.: Prediction of electroencephalographic spectra from neurophysiology. Phys. Rev. E **63**, 1–18 (2001), doi:10.1103/PhysRevE.63.021903

51. Robinson, P.A., Wright, J.J., Rennie, C.J.: Synchronous oscillations in the cerebral cortex. Phys. Rev. E **57**, 4578–4588 (1998), doi:10.1103/PhysRevE.57.4578

52. Scholl, D.A.: The Organization of the Cerebral Cortex. Wiley, New York (1956)

53. Singer, W.: Putative functions of temporal correlations in neocortical processing. In: C. Koch, J.L. Davis (eds.), Large Scale Neuronal Theories of the Brain, MIT Press, Cambridge Mass., London (1994)

54. Singer, W., Gray, C.M.: Visual feature integration and the temporal correlation hypothesis. Annu. Rev. Neurosci. **18**, 555–586 (1995), doi:10.1146/annurev.ne.18.030195.003011

55. Steriade, M., Timofeev, I., Grenier, F.: Natural waking and sleep states: A view from inside cortical neurons. J. Neurophysiol. **85**, 1969–1985 (2001)

56. Steyn-Ross, D.A., Steyn-Ross, M.L., Sleigh, J.W., Wilson, M.T., Gillies, I.P., Wright, J.J.: The sleep cycle modelled as a cortical phase transition. J. Biol. Phys. **31**, 547–569 (2005), doi:10.1007/s10867-005-1285-2

57. Stryker, M.P.: Is grandmother an oscillation? Nature **388**, 297–298 (1989), doi:10.1038/338297a0

58. Stuart, G.J., Sakmann, B.: Active propagation of somatic action potentials into neocortical cell pyramidal dendrites. Nature **367**, 69–72 (1994), doi:10.1038/367069a0

59. Suffczynski, P., Kalitzin, S., Pfurtscheller, G., Lopes da Silva, F.H.: Computational model of thalamocortical networks: Dynamical control of alpha rhythms in relation to focal attention. Int. J. Psychophysiol. **43**, 25–40 (2001), doi:10.1016/S0167-8760(01)00177-5

60. Szentagothai, J.: Local neuron circuits of the neocortex. In: F. Schmitt, F. Worden (eds.), The Neurosciences 4th Study Program, pp. 399–415, MIT Press, Cambridge, Mass (1979)

61. Thomson, A.M.: Activity dependent properties of synaptic transmission at two classes of connections made by rat neocortical pyramidal neurons in vitro. J. Physiol. **502**, 131–147 (1997), doi:10.1111/j.1469-7793.1997.131bl.x

62. Thomson, A.M., West, D.C., Hahn, J., Deuchars, J.: Single axon IPSPs elicited in pyramidal cells by three classes of interneurones in slices of rat neocortex. J. Physiol. **496**, 81–102 (1996)

63. Traub, R.D., Whittington, M.A., Stanford, I.M., Jeffereys, J.G.R.: A mechanism for generation of long-range synchronous fast oscillations in the cortex. Nature **383**, 621–624 (1996), doi:10.1038/383621a0

64. Tsukada, M., Aihara, T., Saito, H.: Hippocampal LTP depends on spatial and temporal correlation of inputs. Neural Netw. **9**, 1357–1365 (1996), doi:10.1016/S0893-6080(96)00047-0

65. Tsukada, M., Yamazaki, Y., Kojima, H.: Interaction between the spatio-temporal learning rule (STLR) and Hebb in single pyramidal cells in the hippocampal CA1 area. Cogn. Neurodyn. **1**, 305–316 (2007), doi:10.1007/s11571-006-9014-5

66. van Rotterdam, A., Lopes da Silva, F.H., van den Ende, J., Viergever, M.A., Hermans, A.J.: A model of the spatio-temporal characteristics of the alpha rhythm. Bull. Math. Biol. **44**, 283–305 (1982), doi:10.1016/S0092-8240(82)80070-0

67. von der Malsburg, C.: How are nervous structures organised? In: E. Basar (ed.), Synergetics of the Brain, Springer, Berlin, Heidelberg, New York (1983)

68. Wilson, H.R., Cowan, J.D.: A mathematical theory of the functional dynamics of cortical and thalamic nervous tissue. Kybernetik **13**, 55–80 (1973), doi:10.1007/BF00288786

69. Wright, J.J.: Reticular activation and the dynamics of neuronal networks. Biol. Cybern. **62**, 289–298 (1990), doi:10.1007/BF00201443

70. Wright, J.J.: Cortical phase transitions: Properties demonstrated in continuum simulations at mesoscopic and macroscopic scales. J. New Math. Nat. Comput. **(in press)** (2009)

71. Wright, J.J.: Generation and control of cortical gamma: Findings from simulation at two scales. Neural Netw. **(in press)** (2009)

72. Wright, J.J., Alexander, D.M., Bourke, P.D.: Contribution of lateral interactions in V1 to organization of response properties. Vision Res. **46**, 2703–2720 (2006), doi:10.1016/j.visres.2006.02.017

73. Wright, J.J., Bourke, P.D.: An outline of functional self-organization in V1: Synchrony, stlr and hebb rules. Cogn. Neurodyn. **2**, 147–157 (2008), doi:10.1007/s11571-008-9048-y

74. Wright, J.J., Bourke, P.D., Chapman, C.L.: Synchronous oscillation in the cerebral cortex and object coherence: Simulation of basic electrophysiological findings. Biol. Cybern. **83**, 341–353 (2000), doi:10.1007/s004220000155

75. Wright, J.J., Liley, D.T.J.: Dynamics of the brain at global and microscopic scales. Neural networks and the EEG. Behav. Brain Sci. **19**, 285–320 (1996)

76. Wright, J.J., Rennie, C.J., Lees, G.J., Robinson, P.A., Bourke, P.D., Chapman, C.L., Gordon, E., Rowe, D.L.: Simulated electrocortical activity at microscopic, mesoscopic, and global scales. Neuropsychopharmacol. **28**, 80–93 (2003), doi:10.1038/sj.npp.1300138

77. Wright, J.J., Sergejew, A.A.: Radial coherence, wave velocity and damping of electrocortical waves. Electroencephalogr. Clin. Neurophysiol. **79**, 403–412 (1991), doi:10.1016/0013-4694(91)90205-I